

Mixed quantitative/qualitative modeling and simulation of the cardiovascular system

Angela Nebot ^{a,*}, François E. Cellier ^b, Montserrat Vallverdú ^c

^a *Llenguatges i Sistemes Informàtics, Universitat Politècnica de Catalunya, Mòdul C6—Campus Nord, Jordi Girona Salgado, 1-3, Barcelona 08034, Spain*

^b *Department of Electrical and Computer Engineering, The University of Arizona, Tucson, AZ 85721, USA*

^c *Institut de Cibernètica, Universitat Politècnica de Catalunya, Diagonal 647, 2na. planta, Barcelona 08028, Spain*

Received 15 February 1996; received in revised form 5 May 1997; accepted 4 September 1997

Abstract

The cardiovascular system is composed of the hemodynamical system and the central nervous system (CNS) control. Whereas the structure and functioning of the hemodynamical system are well known and a number of quantitative models have already been developed that capture the behavior of the hemodynamical system fairly accurately, the CNS control is, at present, still not completely understood and no good deductive models exist that are able to describe the CNS control from physical and physiological principles. The use of qualitative methodologies may offer an interesting alternative to quantitative modeling approaches for inductively capturing the behavior of the CNS control. In this paper, a qualitative model of the CNS control of the cardiovascular system is developed by means of the fuzzy inductive reasoning (FIR) methodology. FIR is a fairly new modeling technique that is based on the general system problem solving (GSPS) methodology developed by G.J. Klir (Architecture of Systems Problem Solving, Plenum Press, New York, 1985). Previous investigations have demonstrated the applicability of this approach to modeling and simulating systems, the structure of which is partially or totally unknown. In this paper, five separate controller models for different control actuations are described that have been identified independently using the FIR methodology. Then the loop between the hemodynamical system, modeled by means of differential equations, and the CNS control, modeled in terms of five FIR models, is closed, in order to study the behavior of the cardiovascular system as a whole. The model described in this paper has been validated for a single patient only. © 1998 Elsevier Science Ireland Ltd. All rights reserved.

Keywords: Cardiovascular system; Inductive reasoning; Fuzzy systems; Quantitative/qualitative modeling

* Corresponding author. Tel.: +34 3 4015642; fax: +34 3 4017014; e-mail: angela@si.upc.es

CARDIOVASCULAR SYSTEM

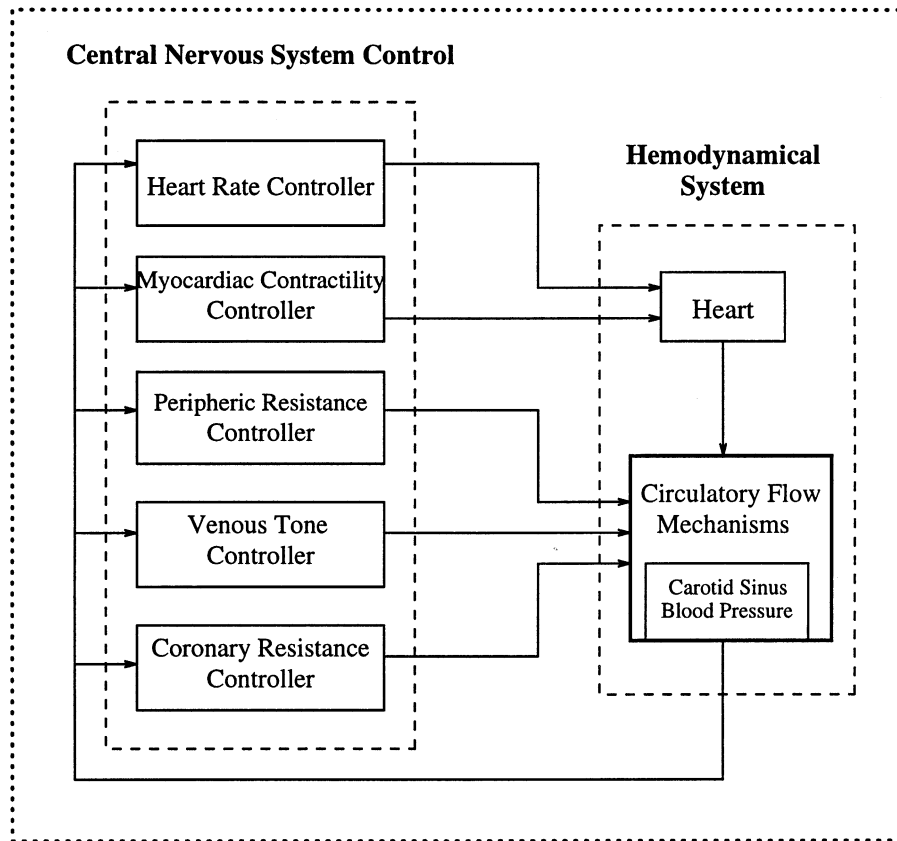


Fig. 1. Simplified diagram of the cardiovascular system model, composed of the hemodynamic system and the CNS control.

1. Introduction

In this paper, a model of the human cardiovascular system is described. It consists of a quantitative highly non-linear ordinary differential equation-based detailed model of the hemodynamical system, described earlier in [1], and a qualitative inductive reasoning-based model of the central nervous system (CNS) control, developed in this paper. A simplified diagram of the cardiovascular system is shown in Fig. 1.

As the hemodynamic model is not central to the research effort discussed in this paper, it is only briefly being touched upon in Appendix A to this paper. For more detail, the reader is referred to [1,2].

The overall CNS model is composed of five separate qualitative models describing the heart rate, peripheral resistance, myocardial contractility, venous tone, and coronary resistance controllers to be described in detail in this paper.

The cardiovascular system model has been validated by means of experimental data obtained from patients carrying out so-called Valsalva maneuvers [1]. The measured output variables of the cardiovascular system considered are the right auricular pressure, P_{AD} , the aortic pressure, P_A , the coronary blood flow, F_A , and the heart rate, HR . Patients having been catheterized for a different purpose were asked whether they would agree to perform several Valsalva maneuvers for the purpose of this study. The Valsalva manoeuvre was chosen because, under this scenario, all con-

trol mechanisms that pertain to the central nervous system control operate in a significant way, causing hemodynamical changes in a short time span.

The four phases that comprise the Valsalva maneuver are usually referred to as phases I, II, III, and IV. Phase I occurs just after the onset of the maneuver, phase II takes place just before the effort is concluded, phase III corresponds to the ending of the maneuver, and finally, phase IV occurs shortly after the maneuver has been completed. The model validation is done by comparing the four simulated output variables with the same quantities available from measurements prior to the onset of the Valsalva maneuver (the Pre-Valsalva phase), as well as during phases II and IV of the Valsalva maneuver.

The qualitative modeling methodology used in the research described in this paper is the fuzzy inductive reasoning (FIR) approach that had first been reported in [3]. Another biomedical application of this modeling methodology for the purpose of modeling the control of an anaesthetic agent (isoflurane) was previously reported in [4]. FIR proved to be excellently suited for modeling observed input/output behavior of systems for which no quantitative model is available. FIR models are synthesized rather than trained, which drastically speeds up the modeling phase in comparison with other inductive modeling techniques, such as neural networks (NN) or NARMAX (Nonlinear AutoRegressive Moving Average with eXternal inputs). The models obtained by the FIR methodology are characterized by a high quality of their predictions. In addition, the methodology offers an important self-assessment capability that prevents it from overgeneralizing, i.e. from making predictions that are not justified on the basis of the available facts.

In this paper, the FIR models will be compared with NARMAX models obtained for the same five subsystems, and the two modeling methodologies will be compared with each other.

The models described in this paper have been validated for a single patient only. No attempts have been made to achieve a generalization that would allow the models to be used for other patients as well. This facet of the research effort

will be reported in a separate publication at some later time.

2. The cardiovascular system

2.1. The hemodynamical system

Over the years, the mathematical models describing the hemodynamical system have grown in size and complexity, proportional to the computational capacity of the available computers and progress made in cardiovascular system clinical research. Elaborate models of the arterial, vein, and cardiac systems that together form the hemodynamical system have been developed by researchers such as Beneken, Rideout, Sagawa, and Snyder [5–7]. They are in compliance with the laws of fluid mechanics.

A recent, and very detailed, hemodynamical model was developed in [2], and more recently reported in [1]. In this model, the heart is composed of four chambers, modeled from the relations between pressure, volume, and elasticity variables. This model is primarily influenced by the publications of Leaning et al. [8], as well as Suga and Sagawa [9]. A summary of the hemodynamical model used in the research reported in this paper is presented in Appendix A to this paper.

The hemodynamical system has been widely studied, and its mechanisms are quite well understood. They are not fundamentally different from those of a hydro-mechanical pump. However, there exist much larger parameter variations from one specimen to the next than would be the case among hydro-mechanical pumps.

It does not make much sense to use a qualitative methodology to identify a hemodynamical model, since no new knowledge can be acquired in this way. The available quantitative models offer a fairly high degree of internal validity, and are therefore suitable for the task at hand. Consequently, the quantitative hemodynamical model presented in [2], described through a set of highly non-linear ordinary differential equations, has been adopted in this study.

2.2. The central nervous system control

The central nervous system controls the hemodynamical system, by generating the regulating signals for the blood vessels and the heart. These signals are transmitted through bundles of sympathetic and parasympathetic nerves, producing stimuli in the corresponding organs and other body parts.

The functioning of the central nervous system is of high complexity and not yet fully understood. This is the reason why many of the cardiovascular system models developed so far have been designed without taking into account the effects of CNS control.

Although the central nervous system control is, at present, still not completely understood, individual differential equation models for each of the hypothesized control mechanisms have been postulated by various authors [8,10,11]. However, these models offer a considerably lower degree of internal validity in comparison with the models used to describe the hemodynamical system.

The use of inductive modeling techniques with their reduced explanatory power but enhanced flexibility for properly reflecting the input/output behavior of a system may offer an attractive alternative to these differential equation models. Furthermore, as shall be shown in this paper, they may offer a self-assessment capability that makes some of these models more robust than the differential equation models. This is particularly true for the FIR methodology advocated in this article.

It is the aim of this paper to apply the FIR methodology to find a qualitative model of the CNS control that accurately represents the input/output behavioral patterns of the CNS control that are available from observations of a particular patient.

The work described in [2] was taken as a starting point. In the research effort reported in [2], two separate CNS control models, a differential equation model and a NARMAX model were developed. The differential equation model represents an enhancement of many individual previous research efforts described by various authors [2,5–7,9,12], and represents one of the most com-

plete deductive CNS control descriptions currently available. The NARMAX model is an inductive model that shares many of the advantages and shortcomings of NN models. Just like the NN models, the NARMAX model is basically a quantitative model with slow training capabilities but easy adaptation possibilities. Neither NN nor NARMAX models have any inbuilt self-validation capabilities. They will predict output values even when presented with input stimuli for which they have not been trained.

The signals obtained from the simulation of the CNS control modeled with differential equations were used by Vallverdú as initial data for the identification of NARMAX models for a set of different patients. These NARMAX models share the same structure for each of the identified patients, but are characterized by different parameter values. The same signals were also used as initial data for the identification of the five FIR models for a single patient.

The CNS control model is composed of five separate controllers: the heart rate controller (HRC), the peripheral resistance controller (PRC), the myocardial contractility controller (MCC), the venous tone controller (VTC), and the coronary resistance controller (CRC). All five controller models are single-input/single-output (SISO) models driven by the same input variable, namely the carotid sinus pressure as shown in Fig. 1. However, the carotid sinus pressure was not one of the measured variables. It is a variable that has been extracted from the differential equation model describing the hemodynamics of the cardiovascular system.

The five output variables of the controller models are not even amenable to a physiological interpretation, except for the HRC variable, which is the inverse heart rate, measured in seconds between beats.

Why were these variables chosen as the interface points between the quantitative and qualitative parts of the model? Would it not have been more meaningful to rely on measured quantities as interface variables? The answer to the last question must clearly be yes! It would have made more sense to proceed in this way. However, by the time this research started, measurements had

already been made, and the structure of the overall model with its decomposition into a hemodynamical and a CNS subsystem including the interface variables as shown in Fig. 1 had already been determined. Under those circumstances, it was deemed more reasonable to continue with the previously established model structure, because this approach allowed us to inherit the hemodynamics model without need for a further modification, made new measurements unnecessary, and furthermore enabled us to compare our results with those obtained previously.

Clearly, the drawback of this solution is the fact that the qualitative models must rely on the previously made differential equation model, and therefore, it cannot be expected that the FIR models will perform better than the differential equation models on which they are based. However, it is important to notice that this drawback is not a deficiency of the proposed methodology itself, only one of the adopted model structure as it refers to the unmeasured and even non-physical character of the interface variables between the quantitative and qualitative parts of the overall model.

It is always a virtue to work with the simplest models possible that explain the available data in order to make potentially necessary patient-specific adjustments to the models as quick and painless as possible. It serves no purpose whatsoever to carry in the models highly sophisticated parameters that are conceptually satisfying, the values of which are, however, impossible to determine either through direct measurements or through indirect parameter identification techniques. The NARMAX models are extremely simple in their internal structure, and therefore satisfy the requirement for simple models. The FIR models are less simple, but they are non-parametric anyway, and setting up a new FIR model can be done easily and quickly. Both types of inductive models are much more manageable than the differential equation model, they were derived from.

The input and output signals of the CNS control, shown in Figs. 2 and 3, have been recorded with a sampling rate of 0.12 s from simulations of the purely differential equation model. The model had been tuned to represent a specific patient

suffering from at least 70% coronary arterial obstruction, by making the four different physiological variables: right auricular pressure, aortic pressure, coronary blood flow, and heart rate of the simulation model agree with the measurement data taken from the patient.

In the modeling process, the normalized mean square error (in percentage) between the simulated output, $\hat{y}(t)$, and the system output, $y(t)$, is used to determine the validity of each of the models. The error equation is given in Eq. (1).

$$\text{MSE} = \frac{E[(y(t) - \hat{y}(t))^2]}{y_{\text{var}}} \cdot 100\% \quad (1)$$

where y_{var} is the variance defined as:

$$y_{\text{var}} = E[y^2(t)] - \{E[y(t)]\}^2 \quad (2)$$

This error measure will also be used to compare the quality of the models obtained for a single patient using the NARMAX and FIR methodologies.

3. The FIR methodology

The FIR methodology is based on the general system problem solver (GSPS) [13], a tool for general system analysis that allows to study the conceptual modes of behavior of dynamical systems. FIR is a qualitative modeling and simulation methodology that is based on observation of input/output behavior of the system to be modeled, rather than on structural knowledge about its internal composition. FIR has two main tasks. The first task is to identify qualitative causal relations between the system variables that are available from observations. In this task, a qualitative model of the observed system is being constructed. The second task is to predict the future behavior of the system from past observations. In this task, the previously constructed model is being used in a qualitative simulation. FIR is a powerful technique, suitable for modeling and simulating systems, for which no or only very limited a priori structural knowledge is available, such as in biomedicine, biology, and the economy.

Fig. 4 shows the two main tasks of the FIR methodology in a schematic way, namely the

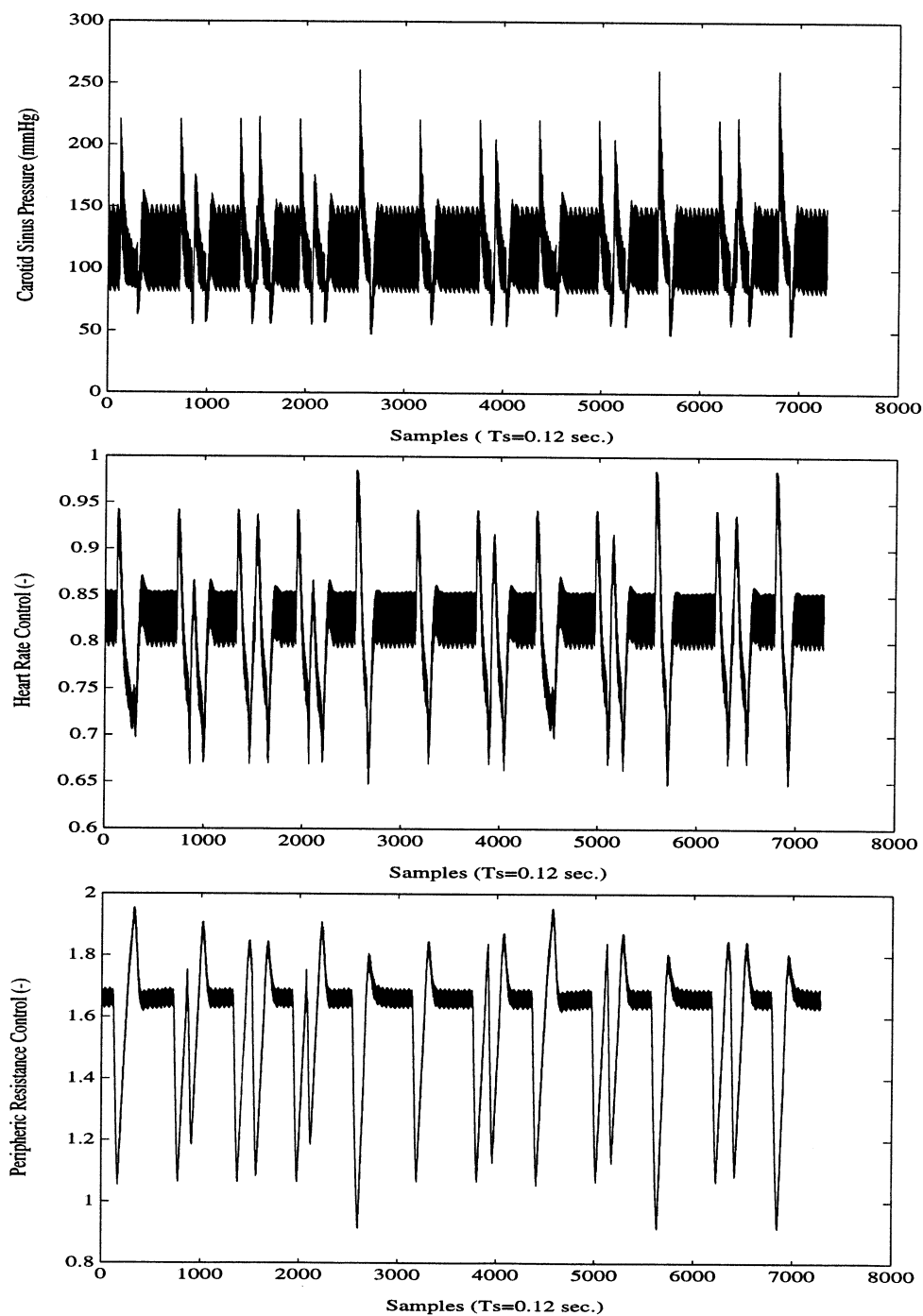


Fig. 2. Carotid sinus pressure, heart rate, and peripheric resistance control signals used to obtain inductive NARMAX and FIR models.

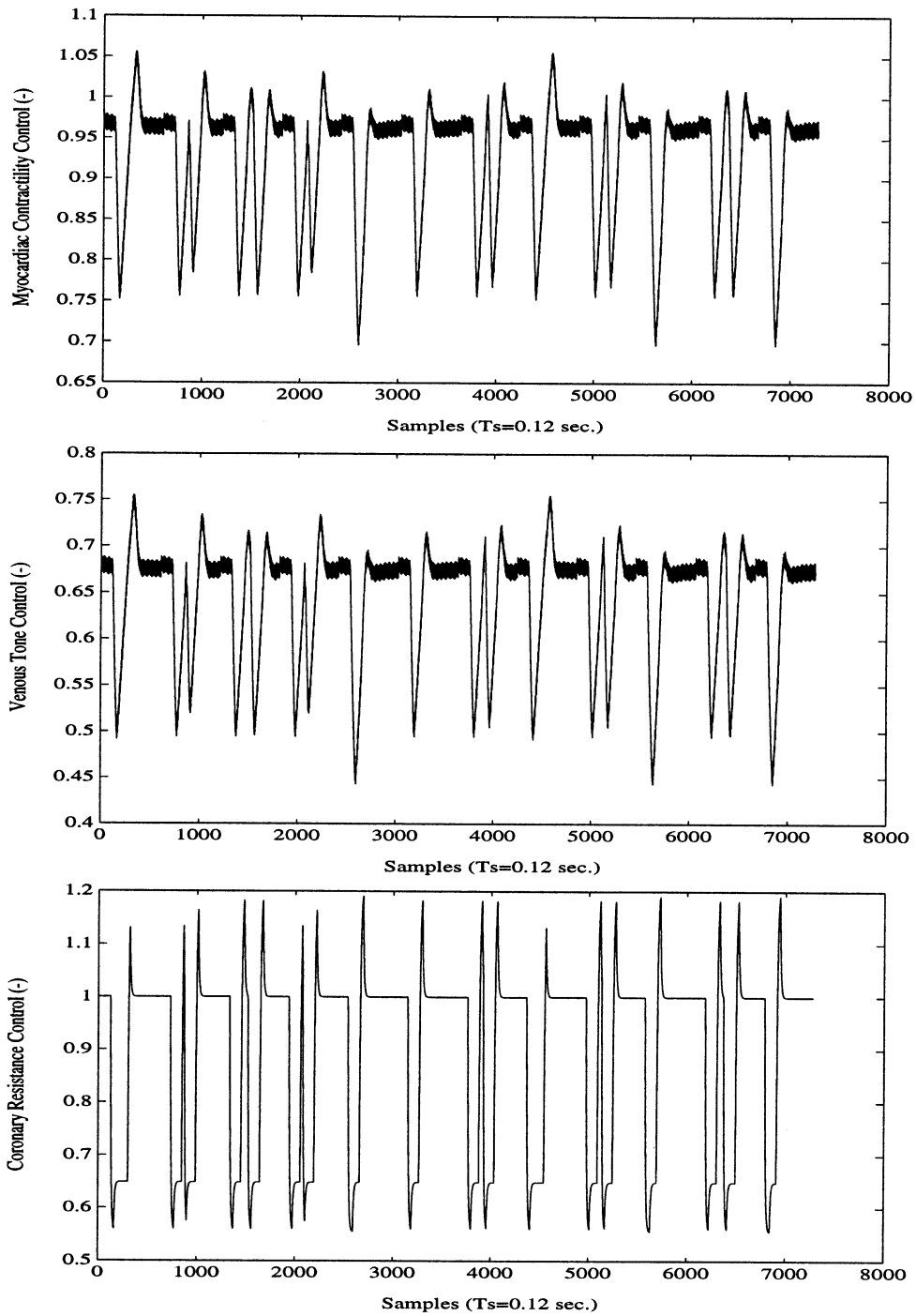


Fig. 3. Myocardial contractility, venous tone, and coronary resistance control signals used to obtain inductive NARMAX and FIR models.

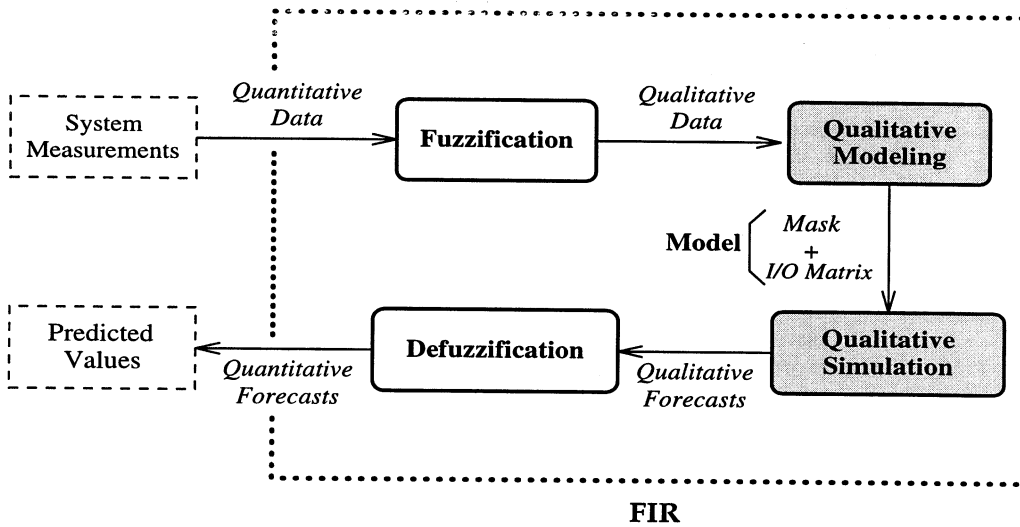


Fig. 4. Schematic representation of the two primary engines of the FIR methodology: qualitative modeling and qualitative simulation, as well as of the two interface engines: fuzzification and defuzzification.

identification of a qualitative model, and the use of that model in a qualitative simulation for the purpose of predicting future behavior of the system under study.

The FIR is fed with data that are measured from the system under study. These are usually quantitative, i.e. real-valued time-stamped data, such as blood pressure, body temperature, etc. However, FIR bases its decisions on qualitative, i.e. discretized, data. Consequently, the measurement data must first be converted from quantitative to qualitative data streams. In order not to lose information in this process, the discretization is not done in a crisp, but rather in a fuzzy sense. In Fig. 4, this process is called fuzzification.

The predictions made by the qualitative simulation engine of FIR are qualitative predictions. It may be desirable to use these predictions subsequently as driving functions (inputs) to a quantitative model. To this end, the qualitative predictions need to be converted back to quantitative data streams. This is accomplished by the defuzzification engine shown in Fig. 4.

The four engines that comprise the FIR methodology are described in more detail in the subsequent sections of this paper.

3.1. Fuzzification

The fuzzification engine converts quantitative values into qualitative triples. The first element of the triple is the class value, the second element is the fuzzy membership value, and the third element is the side value. The class value represents a coarse discretization of the original real-valued variable. The fuzzy membership value denotes the level of confidence expressed in the class value chosen to represent a particular quantitative value. Finally, the side value indicates whether the quantitative value is to the left or to the right of the peak value of the associated membership function. The side value, which is a specialty of the FIR technique since it is not commonly used in fuzzy logic, is responsible for preserving, in the qualitative triple, the complete knowledge that had been contained in the original quantitative value. Fig. 5 illustrates the process of fuzzification by means of an example. A temperature of 23°C would hence be fuzzified into the class 'normal' with a side value of 'right' and a fuzzy membership value of 0.89.

Most fuzzy inferencing approaches preserve the total knowledge by associating with each quantitative data value multiple fuzzy rules consisting of

tuples of class and membership values. They would thus represent the temperature of 23°C as being ‘normal’ with likelihood 0.89 and being ‘warm’ with likelihood 0.05. FIR accomplishes the same by associating with each quantitative data value a single fuzzy rule consisting of a qualitative triple.

In the current implementation of the FIR methodology, in the form of a Matlab [14] toolbox called SAPS-II [3], class values are represented by positive integers, i.e. in the above temperature example, by the numbers ‘1’ representing ‘cold’, ‘2’ denoting ‘fresh’, ‘3’ symbolizing ‘normal’, ‘4’ standing for ‘warm’, and ‘5’ mapping ‘hot’. Similarly, the side values are implemented as ‘-1’ instead of ‘left’, ‘0’ representing ‘center’, and ‘+1’ corresponds to ‘right’. In the continuation of this paper, we shall make use of the numeric representations of these quantities, especially in formulae.

3.2. Qualitative modeling

The qualitative behavior is stored in a qualitative data model. It consists of three matrices of identical sizes, one containing the class values, the second storing the membership information, and the third recording the side values. Each column represents one of the observed variables, and each row denotes one time point, i.e. one recording of all variables, or one recorded state.

In the process of modeling, it is desired to discover finite automata relations among the class values that make the resulting state transition matrices as deterministic as possible. If such a

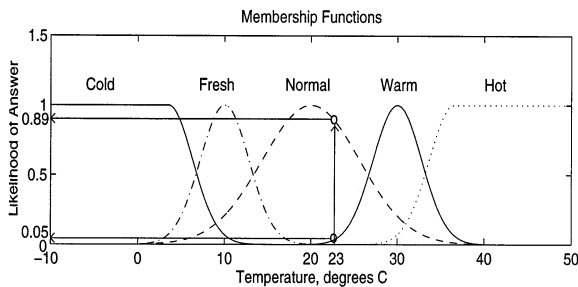


Fig. 5. Gaussian membership functions of a quantitative variable representing ambient temperature.

relationship is found for every output variable, the behavior of the system can be forecast by iterating through the state transition matrices. The more deterministic the state transition matrices are, the higher is the likelihood that the future system behavior will be predicted correctly.

A possible relation among the qualitative variables of a five-variable system example could be of the form:

$$y_1(t) = \tilde{f}(y_3(t - 2\delta t), u_2(t - \delta t), y_1(t - \delta t), u_1(t)) \quad (3)$$

where \tilde{f} denotes a qualitative relationship. Notice that \tilde{f} does not stand for any (known or unknown) explicit formula relating the input arguments to the output argument, but only represents a generic causality relationship that, in the case of the FIR methodology, will be encoded in the form of a tabulation of likely input/output patterns, i.e. a state transition matrix.

In SAPS-II, Eq. (3) is represented by the following so-called ‘mask’ matrix:

$$\begin{matrix} t/x & u_1 & u_2 & y_1 & y_2 & y_3 \\ t - 2\delta t & \left(\begin{matrix} 0 & 0 & 0 & 0 & -1 \\ 0 & -2 & -3 & 0 & 0 \\ -4 & 0 & +1 & 0 & 0 \end{matrix} \right) \end{matrix} \quad (4)$$

The negative elements in this matrix are referred to as *m*-inputs. *m*-inputs denote input arguments of the qualitative functional relationship. They can be either inputs or outputs of the subsystem to be modeled, and they can have different time stamps. The above example contains four *m*-inputs. The sequence in which they are enumerated is immaterial. They are usually enumerated from left to right and top to bottom. The single positive value denotes the *m*-output. The terms *m*-input and *m*-output are used in order to avoid a potential confusion with the inputs and outputs of the system. In the above example, the first *m*-input, i_1 , corresponds to the output variable y_3 two sampling intervals back, $y_3(t - 2\delta t)$, whereas the second *m*-input refers to the input variable u_2 one sampling interval into the past, $u_2(t - \delta t)$, etc.

In the FIR methodology, such a representation is called a mask. A mask denotes a dynamic relationship among qualitative variables. A mask

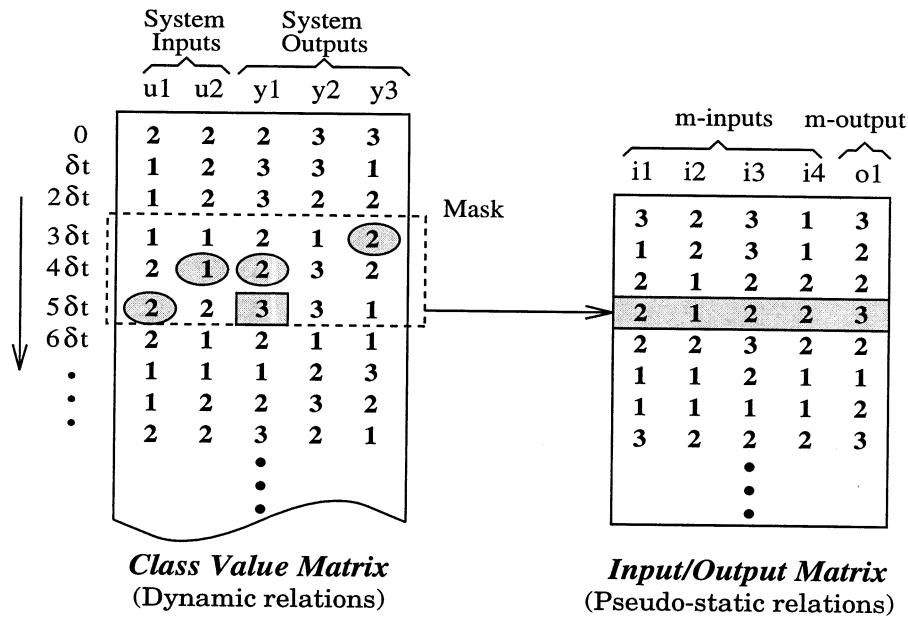


Fig. 6. Process of flattening dynamic relationships into pseudo-static relationships using a mask.

has the same number of columns as the qualitative behavior to which it should be applied, and it has a certain number of rows, the depth of the mask. The mask can be used to ‘flatten’ dynamic relationships into ‘pseudo-static’ relationships. This process is illustrated in Fig. 6. The left side of Fig. 6 shows an excerpt of the class value matrix, one of the three matrices belonging to the qualitative data model. It shows the numerical rather than the symbolic class values. In the example shown in Fig. 6, the first and second variables, u_1 and u_2 , were discretized into two classes, whereas the remaining variables, y_1 , y_2 , and y_3 have been discretized into three classes each. The dashed box symbolizes the mask that is shifted downwards along the class value matrix. The round shaded ‘holes’ in the mask denote the positions of the m -inputs, whereas the square shaded ‘hole’ indicates the position of the m -output. The class values are read out from the class value matrix through the ‘holes’ of the mask, and are placed next to each other in the input/output matrix that is shown on the right side of Fig. 6. Here, each row represents one position of the mask along the class value matrix. It is lined up

with the bottom row of the mask. Each row of the input/output matrix represents one pseudo-static qualitative state or qualitative rule. For example, the shaded rule of Fig. 6 can be read as follows: If the first m -input, i_1 , has a value of ‘2’ (corresponding to ‘medium’), and the second m -input, i_2 , has a value of ‘1’ (corresponding to ‘low’), and the third m -input, i_3 , has a value of ‘2’ (corresponding to ‘medium’), and the fourth m -input, i_4 , has a value of ‘2’ (here corresponding to ‘high’), then the m -output, o_1 , assumes a value of ‘3’ (corresponding to ‘high’).

The qualitative rules can be invoked during qualitative simulation to predict new qualitative outputs. Clearly, these rules can be written in any order, i.e. the sequencing of the rows of the input/output matrix has become irrelevant. They can be sorted alphanumerically. The sorted input/output matrix is called state transition matrix.

From the way, in which the state transition matrix is constructed, it is clear that the same input pattern, a so-called input state can be associated with different output values, i.e. a different output state. If the relationship between input states and output states is non-deterministic, there

will be uncertainty associated with predictions made. Thus, it is advantageous to make the state transition matrix as deterministic as possible.

How is a mask found that, within the framework of all allowable masks, represents the most deterministic state transition matrix, i.e. optimizes the predictiveness of the model? In SAPS-II, the concept of a mask candidate matrix has been introduced. A mask candidate matrix is an ensemble of all possible masks from which the best is chosen by either a mechanism of exhaustive search of exponential complexity [3] or by one of various suboptimal search strategies of polynomial complexity as described in [15,16]. The mask candidate matrix contains ‘-1’ elements where the mask has a potential m -input, a ‘+1’ element where the mask has its m -output, and ‘O’ elements to denote forbidden connections. Thus, a good mask candidate matrix to determine a predictive model for variable y_1 in a five-variable system example might be:

$$\begin{array}{c}
 t/x \\
 t - 2\delta t \\
 t - \delta t \\
 t
 \end{array}
 \begin{array}{ccccc}
 u_1 & u_2 & y_1 & y_2 & y_3 \\
 \left(\begin{array}{ccccc}
 -1 & -1 & -1 & -1 & -1 \\
 -1 & -1 & -1 & -1 & -1 \\
 -1 & -1 & +1 & 0 & 0
 \end{array} \right)
 \end{array}
 \quad (5)$$

Corresponding mask candidate matrices are used to find predictive models for y_2 and y_3 .

Each of the possible masks is compared to the others with respect to its potential merit, i.e. the degree of determinism associated with the state transition matrix constructed from it. The optimality of the mask is evaluated with respect to the maximization of its forecasting power.

The Shannon entropy measure is used to determine the uncertainty associated with forecasting a particular output state given any legal input state. The Shannon entropy relative to one input state is calculated from the equation:

$$H_i = \sum_{o} p(o | i) \cdot \log_2 p(o | i) \quad (6)$$

where $p(o | i)$ is the ‘conditional probability’ of a certain m -output state o to occur, given that the m -input state i has already occurred. The term probability is meant in a statistical rather than in a true probabilistic sense. It denotes the quotient

of the observed frequency of a particular state divided by the highest possible frequency of that state.

The overall entropy of the mask is then computed as the sum:

$$Hm = - \sum_{vi} p(i) \cdot H_i \quad (7)$$

where $p(i)$ is the probability of that input state to occur. The highest possible entropy H_{max} is obtained when all probabilities are equal, and a zero entropy is encountered for relationships that are totally deterministic.

A normalized overall entropy reduction H_r is defined as:

$$H_r = 1.0 - \frac{H_m}{H_{max}} \quad (8)$$

H_r is obviously a real-valued number in the range between 0.0 and 1.0, where higher values usually indicate an improved forecasting power. The masks with highest entropy reduction values generate forecasts with the smallest amounts of uncertainty.

One problem still remains. The size of the input/output matrix increases as the complexity of the mask grows, and consequently, the number of legal states of the model grows quickly. Since the total number of observed data records remains constant, the frequency of observation of each state shrinks rapidly, and so does the predictiveness of the model. The entropy reduction measure does not account for this problem. With increasing complexity, H_r simply keeps growing. Very soon, a situation is encountered where every state that has ever been observed has been observed precisely once. This obviously leads to a totally deterministic state transition matrix, and H_r assumes a value of 1.0. Yet the predictiveness of the model will be dismal, since in all likelihood already the next predicted state has never before been observed, and that means the end of forecasting. Therefore, this consideration must be included in the overall quality measure.

From a statistical point of view, every state should be observed at least five times [17]. Therefore, an observation ratio, O_r , is introduced as an additional contributor to the overall quality measure [18]:

$$O_r = \frac{5 \cdot n_{5 \times} + 4 \cdot n_{4 \times} + 3 \cdot n_{3 \times} + 2 \cdot n_{2 \times} + n_{1 \times}}{5 \cdot n_{\text{leg}}} \quad (9)$$

where: n_{leg} = number of legal m -input states; $n_{1 \times}$ = number of m -input states observed only once; $n_{2 \times}$ = number of m -input states observed twice; $n_{3 \times}$ = number of m -input states observed thrice; $n_{4 \times}$ = number of m -input states observed four times; $n_{5 \times}$ = number of m -input states observed five times or more. If every legal m -input state has been observed at least five times, O_r is equal to 1.0. If no m -input state has been observed at all (no data are available), O_r is equal to 0.0. Thus, O_r can also be used as a quality measure.

The overall quality of a mask, Q_m , is then defined as the product of its uncertainty reduction measure, H_r , and its observation ratio, O_r :

$$Q_m = H_r \cdot O_r \quad (10)$$

The optimal mask is the mask with the largest Q_m value.

3.3. Qualitative simulation

Once the best model is obtained by means of computing the quality measure presented above, future output states can be predicted using the inference engine that is at the heart of the qualitative simulation module inside FIR. Using the five-nearest-neighbors (5NN) fuzzy inferencing algorithm [3,19], the membership and side functions of the new input are compared with those of all previous recordings of the same qualitative input. The input with the most similar membership and side functions is identified. For this purpose, a normalized defuzzification:

$$\text{pos}_i = \text{class}_i + \text{side}_i \cdot (1.0 - \text{Memb}_i) \quad (11)$$

is computed for every input variable of the new input set, and these pos_i values are stored in a vector, **pos**. The index i represents the i th input variable in the input state of the current observation. Memb_i is the membership value, and class_i and side_i are the numeric class and side values associated to those inputs, respectively. The position value, pos_i , can be interpreted as a normalized defuzzification of the i th input variable. Irrespective of the original values of the input

variable, pos_i assumes values in the range (1.0–1.5) for the lowest class, (1.5–2.5) for the next higher class, etc.

The defuzzification is repeated for all previous recordings of the same input state:

$$\text{pos}_{ij} = \text{class}_{ij} + \text{side}_{ij} \cdot (1.0 - \text{Memb}_{ij}) \quad (12)$$

where the index j denotes the j th previous observation of the same input state. Also the pos_{ij} values are stored in a vector, **pos_j**. Then, the \mathcal{L}_2 norms of the difference between the **pos** vector of the new input state and the **pos_j** vectors of all previous recordings of the same input state are computed:

$$\text{dis}_j = \sqrt{\sum_{i=1}^N (\text{pos}_i - \text{pos}_{ij})^2} \quad (13)$$

where N is the number of m -inputs.

Finally, the previous recording with the smallest \mathcal{L}_2 norm is identified. The class and side values of the output state associated with this input state are then used as forecasts for the class and side values of the new output state.

Forecasting of the new membership function is done a little differently. Here, the five previous recordings with the smallest \mathcal{L}_2 norms are used (if at least five such recordings are found in the input/output matrix), and a distance-weighted average of their fuzzy membership functions is computed and used as the forecast for the fuzzy membership function of the current state. This is done in the following way.

The distances of each of the five nearest neighbors is limited from below by ϵ , the smallest number that is distinguishable from 1.0 in addition:

$$d_j = \max([\text{dis}_j, \epsilon]) \quad (14)$$

s_d is the sum of all d_j values:

$$s_d = \sum_{j=1}^5 d_j \quad (15)$$

Relative distances are then computed as:

$$d_{\text{rel}_j} = \frac{d_j}{s_d} \quad (16)$$

Absolute weights are then computed as follows:

$$w_{\text{abs}_j} = \frac{1.0}{d_{\text{rel}_j}} \quad (17)$$

Using the sum of the absolute weights:

$$s_w = \sum_{j=1}^5 w_{\text{abs}_j} \quad (18)$$

it is possible to compute relative weights:

$$w_{\text{rel}_j} = \frac{w_{\text{abs}_j}}{s_w} \quad (19)$$

The relative weights are numbers between 0.0 and 1.0. Their sum is always equal to 1.0. It is therefore possible to interpret the relative weights as percentages. Using this idea, the membership function of the new output can be computed as a weighted sum of the membership functions of the outputs of the previously observed five nearest neighbors:

$$\text{Memb}_{\text{out}_{\text{new}}} = \sum_{j=1}^5 w_{\text{rel}_j} \cdot \text{Memb}_{\text{out}_j} \quad (20)$$

3.4. Defuzzification

The defuzzification engine of the FIR methodology is responsible for converting each qualitative predicted output triple back to a quantitative output value. It is the inverse operation of the previously described fuzzification engine. Since the qualitative triples retain complete knowledge of the quantitative variables they represent, the defuzzification operation is unambiguous.

In a mixed quantitative and qualitative simulation, the fuzzification and defuzzification modules play the roles of interface points between the quantitative and qualitative submodels.

For a deeper and more detailed insight into the FIR methodology, the reader is referred to [18–21].

4. The qualitative CNS controller models

The method used for deriving the FIR heart rate controller model shall be demonstrated in detail in this paper. Since the other four qualitative controller models are obtained in exactly the same fashion, it does not serve any purpose to

repeat the same explanations several times over. The heart rate controller design can serve as a valid example for all of them. Only the final results obtained shall be given for the other four controllers. Details of their design can be found in [21].

The five controllers that compose the CNS, named heart rate, peripheral resistance, myocardial contractility, venous tone, and coronary resistance controllers are all single-input/single-output (SISO) systems. They all have the carotid sinus pressure as their input variable. They differ in their respective output variables. The common input and the five controller outputs are shown on Figs. 2 and 3.

4.1. FIR model of the heart rate controller

The input and output variables of the heart rate controller subsystem were fuzzified into three qualitative classes each. Three classes are sufficient to obtain a good qualitative model of the system, and consequently, it was not necessary to work with more complex models.

For the heart rate controller, the optimal mask found was the following:

$$\begin{array}{c} t/x \\ t - 2\delta t \\ t - \delta t \\ t \end{array} \begin{array}{cc} \text{CSP} & \text{HRC} \\ \left(\begin{array}{cc} 0 & 0 \\ -1 & -2 \\ -3 & +1 \end{array} \right) \end{array} \quad (21)$$

i.e. although a mask depth of three was initially proposed, the qualitative modeling (optimization) algorithm reduced the mask depth from three to two. The optimal mask denotes the qualitative relationship:

$$\text{HRC}(t) = \tilde{f}(\text{CSP}(t - \delta t), \text{HRC}(t - \delta t), \text{CSP}(t)) \quad (22)$$

Notice that $\delta t = 0.24$, i.e. only every second data point was used by the qualitative model.

The data used in the identification process (Fig. 2) constitute only a subset of the data available from the studied patient. The model was validated by using it to forecast six data sets that had not been employed in the model identification process, i.e. using data that the model had never seen

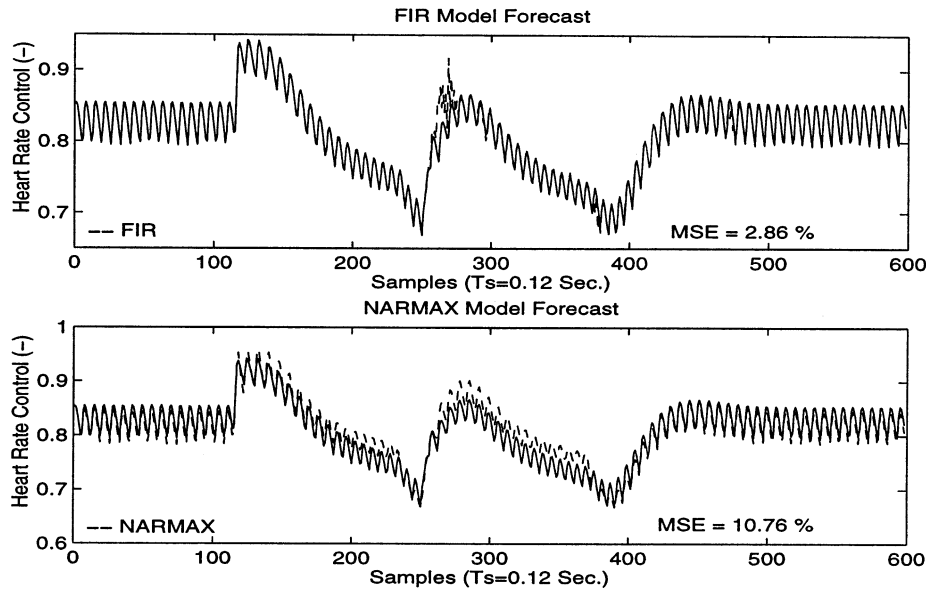


Fig. 7. Heart rate control: FIR worst data set forecast and NARMAX forecast for the same data set.

before. Each one of these six data sets, with a size of about 600 data points each, contains signals representing specific morphologies, allowing the validation of the model for different system behaviors. Data set #1 represents two consecutive Valsalva maneuvers of 10 s duration separated by a 2 s break, data set #2 shows two consecutive Valsalva maneuvers of 10 s duration separated by a 4 s break, and data set #3 exhibits two consecutive Valsalva maneuvers of 10 s duration separated by an 8 s break. Data set #4 shows a single Valsalva maneuver of 10 s duration with an intensity (pressure) increase of 50% relative to the previous three data sets. Data set #5 describes a single Valsalva maneuver of 20 s duration with nominal pressure. Finally, data set #6 characterizes a single Valsalva maneuver of 10 s duration with nominal pressure. Data set #6 is called the reference data set, since it represents a standardized Valsalva maneuver, from which all the other variants are derived by modifying a single parameter.

The upper portion of Fig. 7 shows a comparison of the output obtained by forecasting data set #1 using the FIR model (dashed line) with the true measured output (solid line). The data exhibit

high frequency oscillations modulated onto a low frequency signal. The FIR model is capable of properly forecasting both the low-frequency and the high-frequency behavior of this signal. There is only a short interval where the FIR model evidently was unable to predict how the signal is supposed to continue.

The mean square error (MSE) for this signal is 2.86%. It should be noted that the forecast shown in Fig. 7 is the worst result obtained for any of the six data sets. Since even this forecast is fairly good, the model can be accepted as valid. The mean square errors obtained for the six model validation data sets are given in the HRC column of Table 1. Data sets #5 and #6 lead to almost perfect forecasts. In those cases, the dashed line cannot be distinguished at all from the solid line by the naked eye. Each of the other four data sets contains a short segment where the forecast temporarily is of much lower quality.

4.2. FIR models of the other CNS controllers

The same identification procedure has been used in order to obtain FIR models of the other four controllers. Each of those resulted in a differ-

Table 1
MSE errors obtained for the six validation data sets using FIR to predict the HR, PR, MC, VT and CR control variables

	HRC (%)	PRC (%)	MCC (%)	VTC (%)	CRC (%)
Data set 1	2.86	1.06	2.22	1.77	0.02
Data set 2	1.43	0.03	0.08	0.05	0.04
Data set 3	1.10	2.71	0.16	4.34	0.02
Data set 4	2.61	0.07	0.14	0.55	0.48
Data set 5	0.09	4.88	5.69	1.86	0.01
Data set 6	0.12	0.17	0.20	0.23	0.00
Average Error	1.37	1.49	1.41	1.47	0.09

ent optimal mask. Simulation results of the model validation runs for the other four qualitative controller models are presented in the upper portions of Figs. 8–11. The worst predictions for the peripheral resistance and myocardial contractility controller models were obtained with data set #5. The worst prediction for the venous tone controller was obtained when using data set #3. Finally, the worst behavior was exhibited by the coronary resistance controller when using data set #4. Figs. 8–11 show the worst predictions obtained by each of the five controller models.

The computation of the MSE errors of the peripheral resistance, myocardial contractility, venous tone, and coronary resistance controller models are also presented in Table 1. The table shows that the average errors obtained for the six validation data sets are all smaller than 1.5%. Hence, the FIR qualitative modeling methodology has been shown to work exceedingly well when confronted with cardiac data.

5. Comparisons of NARMAX and FIR controller models

In this section, a comparison of the five controller models obtained for a given patient using two different modeling methodologies is presented. These methodologies are the NARMAX quantitative inductive modeling technique and the previously introduced FIR qualitative inductive modeling technique.

Both methodologies used the same data sets presented in Figs. 2 and 3 for model identifica-

tion. In the model validation process, the same six validation data sets that had previously been described were used by both the NARMAX and FIR methodologies.

5.1. NARMAX models of the CNS controllers

In this section, the NARMAX models of the five controllers that compose the CNS cardiovascular control are described.

The NARMAX model of five terms that best represents the HRC for the given patient is described in Eq. (23).

$$\begin{aligned}
 \text{HRC}(t) &= 0.0346 + 7.9151 \cdot 10^{-4} * \text{CSP}(t) \\
 &+ 0.7612 * \text{HRC}(t-1) + 0.1133 * \text{HRC}(t-7) \\
 &- 1.5930 \cdot 10^{-6} * \text{CSP}(t) * \text{CSP}(t-3) \quad (23)
 \end{aligned}$$

The model shown in Eq. (23) is different from that presented in [2], because it is specialized for the given patient, whereas the model presented in [2] is a more general NARMAX model that can be used to reflect the behavior of a variety of different patients with similar morphologies.

The prediction of this model for the data set #1 is shown in the lower portion of Fig. 7. In the upper portion of the same plot, the forecast results obtained by the corresponding FIR model are presented for the same data set. Hence, a direct comparison between the two graphs can be made.

The NARMAX model follows the low-frequency behavior fairly well, but does not reflect the high-frequency oscillations faithfully. Conse-

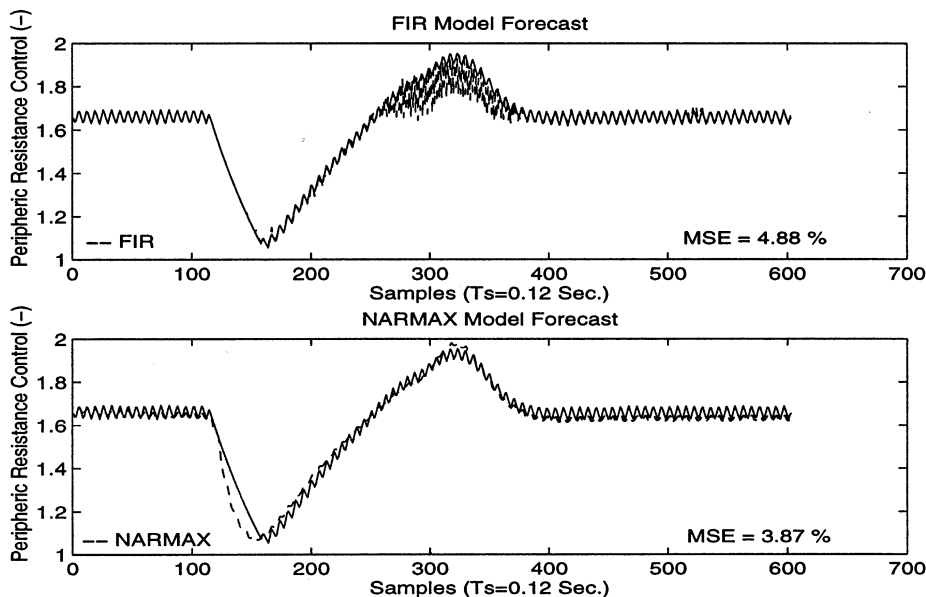


Fig. 8. Peripheric resistance control: FIR worst data set forecast and NARMAX forecast for the same data set.

quently, its MSE error is more than four times as large as that of the corresponding FIR model.

The NARMAX model of three terms that best represents the peripheric resistance control behavior of the given patient is described in Eq. (24).

$$\begin{aligned}
 PRC(t) &= 0.0489 + 0.9851 \cdot PRC(t - 1) \\
 &\quad - 2.0074 \cdot 10^{-6} \cdot CSP(t - 1) \cdot CSP(t - 7) \quad (24)
 \end{aligned}$$

The prediction of this model for data set # 5 is shown in the lower portion of Fig. 8. It should be noted that the upper portion of Fig. 8 shows the worst FIR prediction obtained for any of the six validation data sets, whereas the lower portion shows the best of the NARMAX predictions. This time, the NARMAX model does not make any attempt at predicting the high-frequency component of the signal at all. The FIR model exhibits a fairly large time segment where its prediction is of reduced quality, whereas during the remainder of the time, the prediction is right on the mark.

The NARMAX model of three terms that best represents the myocardial contractility controller is described in Eq. (25).

$$\begin{aligned}
 MCC(t) &= 0.0177 + 0.9897 \cdot MCC(t - 1) \\
 &\quad - 6.5093 \cdot 10^{-7} \cdot CSP(t - 1) \cdot CSP(t - 7) \quad (25)
 \end{aligned}$$

The prediction of this model for data set # 5 is shown in the lower portion of Fig. 9. As in the previous case, data set # 5 corresponds to the worse forecast using the FIR model and to the best forecast using the NARMAX model. Yet, the MSE error is still slightly larger for the NARMAX model than for the FIR model.

The NARMAX model of three terms that best represents the venous tone controller is given in Eq. (26).

$$\begin{aligned}
 VTC(t) &= 0.01374 + 0.9897 \cdot VTC(t - 1) \\
 &\quad - 5.6402 \cdot 10^{-7} \cdot CSP(t - 1) \cdot CSP(t - 7) \quad (26)
 \end{aligned}$$

The prediction of this model for data set # 3 is shown in the lower portion of Fig. 10.

Finally, the NARMAX model of six terms that best represents the coronary resistance controller is shown in Eq. (27).

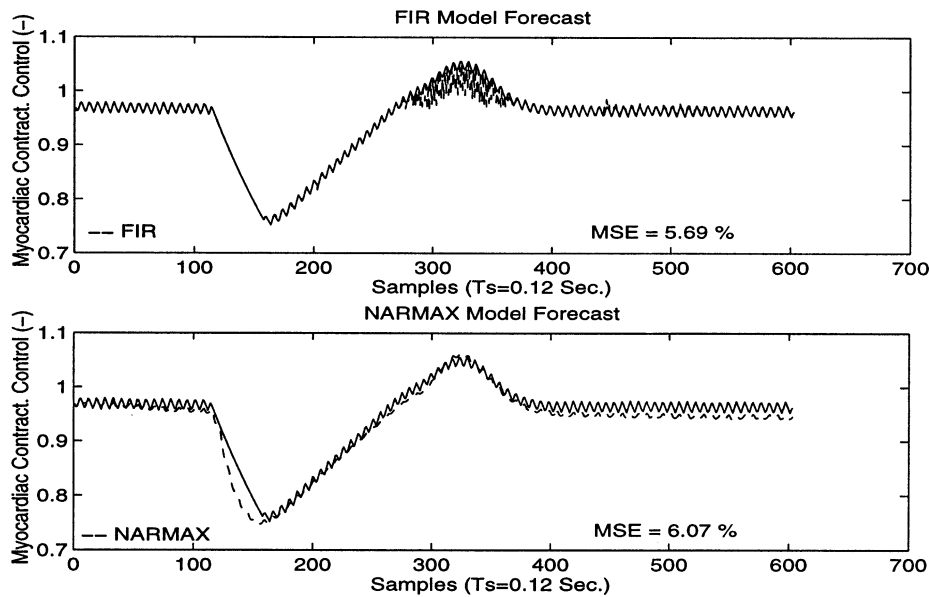


Fig. 9. Myocardial contractility control: FIR worst data set forecast and NARMAX forecast for the same data set.

$$\begin{aligned}
 & \text{CRC}(t) \\
 & = 0.0215 - 4.6999 \cdot 10^{-5} * \text{CSP}(t - 10) \\
 & \quad + 1.0015 * \text{CRC}(t - 1) \\
 & \quad - 9.4519 \cdot 10^{-7} * \text{CSP}(t - 6) * \text{CSP}(t - 8) \\
 & \quad + 3.0283 \cdot 10^{-7} * \text{CSP}(t - 10) * \text{CSP}(t - 10) \\
 & \quad - 1.0381 \cdot 10^{-4} * \text{CSP}(t - 10) * \text{CRC}(t - 1) \quad (27)
 \end{aligned}$$

The prediction of this model for data set #4 is shown in the lower portion of Fig. 11. In this case, the results correspond to the worst forecasts obtained from both the FIR and NARMAX models.

Comparing the FIR and NARMAX models of the five controllers, it becomes evident that the FIR modeling technique provides considerably better results in situations, such as in cardiology, where lots of data are available to train the model with, and where the signals are fairly repetitive in nature.

The normalized mean square errors, MSE, of the five CNS controller models have been computed for each of the six validation data sets

individually, and also for all data sets together. These results are presented in Tables 1 and 2.

Comparing the MSE errors obtained for each controller using the NARMAX models (Table 2) with those obtained using the FIR models (Table 1), it becomes evident that the errors obtained using the FIR models are, on average, much smaller than those obtained by the NARMAX models.

Yet, the NARMAX models are considerably simpler than their FIR rivals, and moreover, NARMAX models can be used to extrapolate behavior, whereas FIR models can only interpolate behavior. Evidently, a FIR model can only predict behavior that it has previously seen in a similar form. Hence, FIR models have very little extrapolative power. However, this property of FIR may in fact be one of the greatest virtues of this methodology. Although they reject to extrapolate beyond the range of previously experienced behavioral patterns, FIR models are considerably more robust and reliable than their NARMAX and differential equation competitors. This issue shall be discussed in more detail in due course.

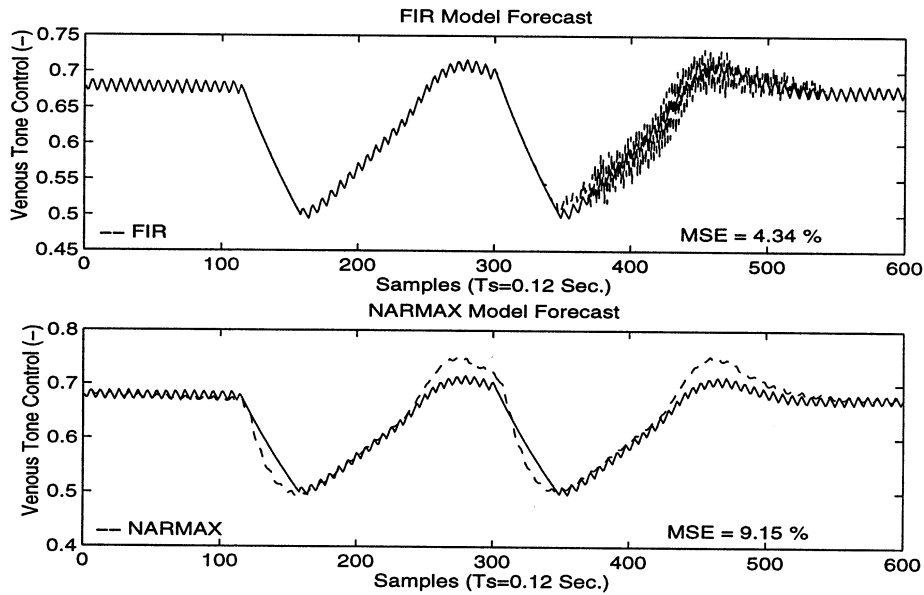


Fig. 10. Venous tone control: FIR worst data set forecast and NARMAX forecast for the same data set.

6. The cardiovascular closed-loop system

In this section, the loop between the hemodynamical system, modeled by means of differential equations, and the central nervous system control, modeled in terms of inductive modeling techniques, is closed. The complex behavior of the overall cardiovascular system is now studied.

Real physiological data obtained from cardiac catheterization are used for this study. These data were obtained from the hemodynamical division of the Hospital de la Santa Creu i de Sant Pau in Barcelona. The data stem from a patient with coronary arterial obstruction of at least 70%. The measured physiological variables are: the right auricular pressure, $P_{AD}(t)$, the aortic pressure, $P_A(t)$, the coronary blood flow, $F_C(t)$, and the heart rate, $HR(t)$. The physiological variables were recorded during all five phases of the Valsalva maneuver.

From the trajectories of the right auricular pressure, the aortic pressure, the coronary blood flow, and the heart rate, mean values were computed for each of the five phases of the maneuver. P_{ADM} denotes the average right auricular pressure during a given phase, P_{AM} stands for the mean

aortic pressure, F_{CM} is the average coronary blood flow, and HR_M signifies the average heart rate during any one of the phases.

The measurement results obtained through cardiac catheterization for the studied patient are summarized in Table 3. Only the mean values computed for the pre-Valsalva phase, the Valsalva phase II, and the Valsalva phase IV are shown in the table, because these are the most significant data.

The mean values presented in the first column of Table 3 were obtained from real measurements. They will consequently be used as reference values in the model validation process. In order for a model to pass the acceptance test, none of the four key variables, i.e. the average right auricular pressure, the mean aortic pressure, the mean coronary blood flow, and the average heart rate must deviate from the reference values by more than $\pm 10\%$ during any of the three key phases of the Valsalva maneuver, i.e. the pre-Valsalva phase, the Valsalva phase II and the Valsalva phase IV.

In [2], two different cardiovascular system models were studied; a model described solely by means of differential equations (second column of Table 3), and another model whose hemodynamical

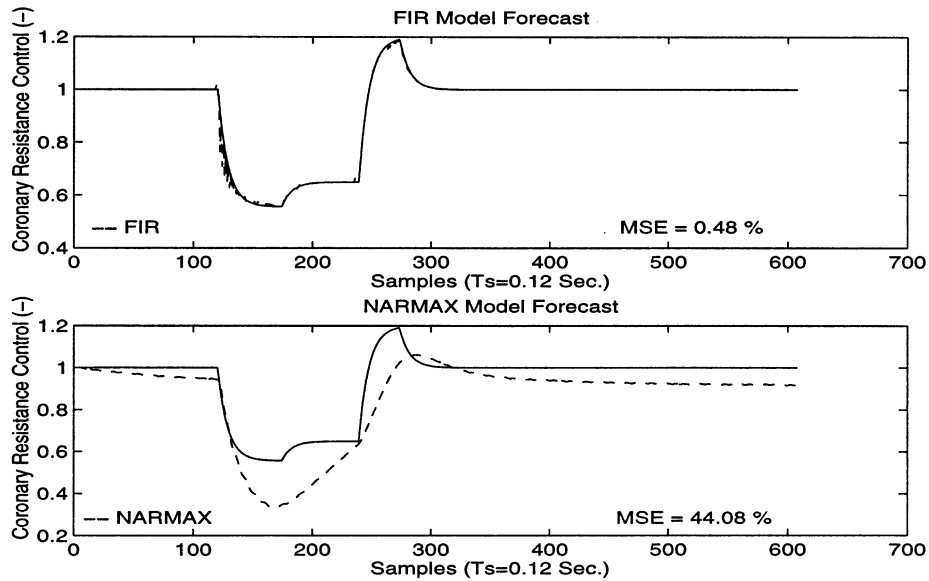


Fig. 11. Coronary resistance control: FIR worst data set forecast and NARMAX forecast for the same data set.

cal subsystem was modeled using differential equations and whose central nervous system control was modeled by means of the NARMAX methodology (fourth column of Table 3).

The simulation results obtained from either of the two cardiovascular system models was found to lie inside the $\pm 10\%$ error margin permitted, and therefore, both models were considered to be valid for the task at hand.

Looking at the results obtained with the purely deductive differential equation model presented in the second column of Table 3, it can be seen that the largest negative relative deviation from the measurement values is -5.19% , whereas the largest positive relative deviation is $+5.93\%$. Thus, all the indicators are clearly within the requested $\pm 10\%$ margin. The average relative deviation from the measurement values is 2.52% .

At this point, the question to be raised is whether a mixed model of the cardiovascular system, whereby the hemodynamical subsystem is described by means of differential equations and the CNS control is described using a FIR model also generates results inside the $\pm 10\%$ error margin permitted and can therefore also be considered a valid model for the task at hand.

The differential equation model of the hemodynamical system was implemented using the advanced continuous simulation language (ACSL) [22], a convenience software tool for the description of ordinary differential equation-based state-space models, whereas the qualitative central nervous system control was realized using SAPS-II [18–21]). ACSL was chosen as the implementation language for the hemodynamical system primarily because an interface between ACSL and SAPS-II had already been developed [3]. A simplified scheme of the simulation structure is shown in Fig. 12.

The hemodynamical system, modeled and simulated in a strictly quantitative fashion, is implemented in full within ACSL. Its differential equations are implemented as a continuous process within ACSL to be integrated across time using one of the standard integration algorithms offered by ACSL. The CNS control, on the other hand, is implemented inside the ACSL program as a discrete process to be executed once every 0.24 s.

The simulation process operates in the following way. The hemodynamical system generates a continuous-time trajectory representing the carotid sinus pressure. This variable is sampled by

Table 2

MSE errors obtained for the six validation data sets using NARMAX to predict the HR, PR, MC, VT and CR control variables

	HRC (%)	PRC (%)	MCC (%)	VTC (%)	CRC (%)
Data set 1	10.77	20.47	20.19	23.67	42.09
Data set 2	7.62	8.62	7.52	8.84	21.02
Data set 3	7.08	9.20	8.18	9.15	19.07
Data set 4	11.64	38.25	51.52	46.90	44.08
Data set 5	13.07	3.88	6.07	3.97	43.03
Data set 6	8.60	8.91	9.77	8.81	20.87
Average Error	9.80	14.89	17.21	16.89	31.69

the discrete process once every 0.24 s and is immediately being fuzzified into three qualitative classes using the SAPS fuzzification engine that is coupled to ACSL through an interface routine. The discrete process then calls five times upon the SAPS fuzzy forecasting routine to predict qualitative values of the five controller outputs. These five qualitative triples are then defuzzified into quantitative (real-valued) controller outputs using the FIR defuzzification engine. The defuzzified signals are then made available to the hemodynamical system for use within the differential equation model. The overall effect of the qualitative CNS control model is that of a single-input multi-output (SIMO) digital controller with sample-and-hold (ZOH) circuitry at each of the five controller outputs. The qualitative processes, fuzzification, prediction, and defuzzification, are executed inside SAPS-II, reducing the ACSL implementation of the CNS control to a mere interface.

The simulation results obtained from the mixed quantitative and qualitative cardiovascular system model using fuzzy inductive reasoning for the description of the CNS control are summarized in the third column of Table 3.

As can be seen from Table 3, the largest negative relative deviation from the measurement values is -5.093% , and the largest positive relative deviation is $+7.79\%$. Thus, all the indicators are again within the requested $\pm 10\%$ margin, and in accordance with the requirements, also this model is to be accepted as a valid representation of reality for the task at hand. The average relative deviation from the measurement values is 2.78% .

Consequently, the average deviation from the measurement data is here a little larger than in the purely deductive differential equation model.

The results obtained from the mixed differential equation and NARMAX model are summarized in the fourth column of Table 3. It is necessary to point out that these results have not been obtained using the specialized NARMAX models presented in the previous section of this paper. These are the results reported in [2], where NARMAX models were identified with a structure common to all patients analyzed. Only the parameters of the NARMAX models were identified for each patient separately.

Here, the largest negative relative deviation from the measurement values is -4.06% , and the largest positive relative deviation is $+6.09\%$. Thus, all the indicators are again within the requested $\pm 10\%$ margin. The average relative deviation from the measurement values is 1.48% . Since the average deviation is a little smaller than in the case of the differential equation model, the mixed differential equation and NARMAX model can be considered to be of higher quality than the pure differential equation model. These results were obtained by post-optimizing the NARMAX model parameters in closed loop to get the best possible fit with the real measurement data.

It should be recalled how the FIR model was created, namely as a replica of the purely quantitative differential equation model, and not as a replica of the measurement data. Comparing the FIR model with the differential equation model, it is found that the largest negative relative deviation between the two models is 0.0% , whereas the

Table 3

Comparison of measurement data of the cardiovascular closed-loop system with simulation results obtained by using the FIR, NARMAX and differential equation CNS control models

		Cathet.	Diff. equal	FIR	NARMAX
P_{ADM}	Pre-V	4	4	4	4
	II	38	38	38	38
	IV	5	5	5	5
P_{AM}	Pre-V	107	111	110	108
	II	99	100	100	99
	IV	119	118	117	117
F_{CM}	Pre-V	123	119	118	128
	II	106	105	105	102
	IV	118	125	125	118
HR_M	Pre-V	77	73	71	76
	II	82	79	78	77
	IV	70	74	73	70

largest positive relative deviation is +2.73%. The average relative deviation between the two models is 0.66%.

This is an impressive similarity. The FIR model replicated exceptionally well what it was told to be the ‘reality’, i.e. the differential equation model.

7. Confidence measure of the FIR methodology

Qualitative forecasting of soft-science systems is quite different from quantitative modeling and simulating of hard-science systems, such as electronic circuits, for example. Whereas highly accurate simulation results can be expected in the latter case, the same does not hold true for the former.

Hence, it is important to always interpret qualitative simulation results with caution and a certain degree of scepticism. That the qualitative simulations turned out so well in the example presented in this paper is only due to the highly repetitive nature of cardiological systems, i.e. to the high degree of redundancy inherent in cardiological measurement data.

Although the request for scepticism is a good mandate on moral grounds, is it also a practical demand? How should the medical practitioner

know how to judge the reliability of a prediction made? He or she has no way of knowing how good the predictions are. Hence, it is important to instil scepticism into the qualitative simulation software itself, rather than demanding it of its users.

It should be a matter of principle that all simulation tools used to predict the behavior of soft-science systems contain a self-assessment capability. In other words, qualitative simulation software should not only forecast the future behavior of a system, but also make a prediction of the confidence that it has in its own prophecies, and/or estimate the errors associated with its predictions.

The NARMAX models presented in this paper have no self-assessment capability at all. Presented with any input sequence, they will present something, irrespective of whether the predictions they make have any bearing on reality or not. The same holds true for the differential equation models.

A self-assessment capability could be instilled into a NARMAX forecasting tool by simulating with multiple NARMAX models in parallel, while comparing the predictions they make with each other. If two forecasts of the same signal are in disagreement, it is clear that at least one of them must be incorrect. However, it is not clear, which

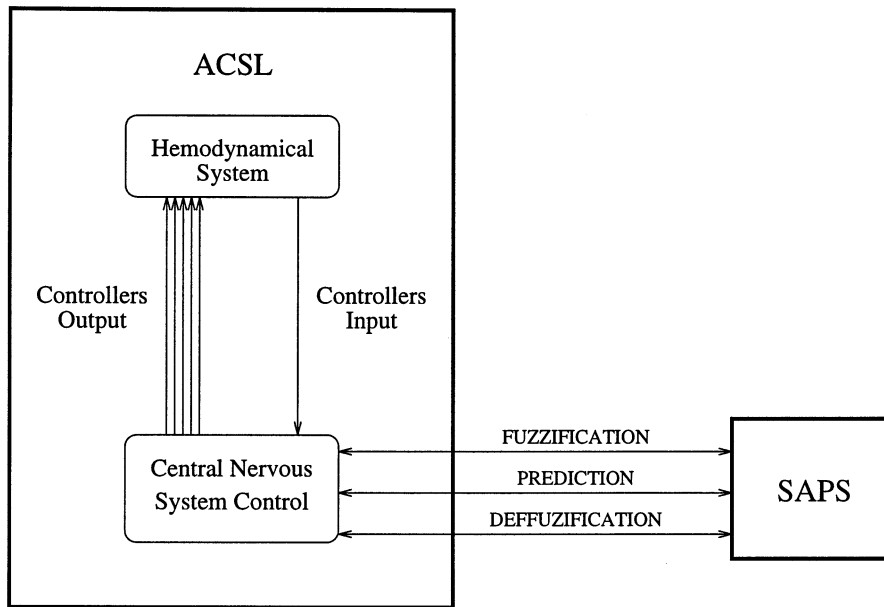


Fig. 12. Schematic showing the structure of the program used to simulate the cardiovascular system.

of them, if any, is the correct one. Moreover, if the two forecasts agree with each other, it could still be that both are equally incorrect. The problem is that any such scheme only provides a relative and not an absolute measure of confidence. The models are only compared to each other rather than being compared to the original data that were used to create these models in the first place.

The FIR methodology operates differently. The qualitative modeling stage only determines the relevance of a set of given data points in the prediction of any output variable, i.e. it rearranges the available measurement data in a smart way for future reference. However, all the measurement data are at the disposal of the qualitative simulation engine. In fact, qualitative simulation simply means to relate the current input pattern to similar patterns observed in the past and stored in the experience data base.

Hence, it is possible to determine the relevance of the data stored in the experience data base to the situation currently at hand. The more relevant the previously stored input patterns are to the current situation, and the more unambiguous the

corresponding outputs are, the more confidence there can be that the same input/output pattern applies to the current situation. This mode of reasoning can be used to determine an absolute measure of confidence, i.e. a confidence measure that relates the currently made prediction to the available facts (the previously observed data), rather than to a model that has been derived from those facts, the validity of which may itself be questionable.

The upper portion of Fig. 13 shows the forecast of data set #5 for the myocardial contractility controller using the FIR model. It can be seen that the prediction is excellent during the early and late parts of the prediction period. However, there is a time segment approximately between samples 270 and 360 where the prediction is rather poor. The lower portion of Fig. 13 shows the local confidence measure computed for the same output variable. It turns out that FIR is perfectly capable of realizing when it is about to make mistakes in its prediction.

The algorithm used for determining the confidence of a prediction is the following. It is based on the same absolute weights of the five nearest

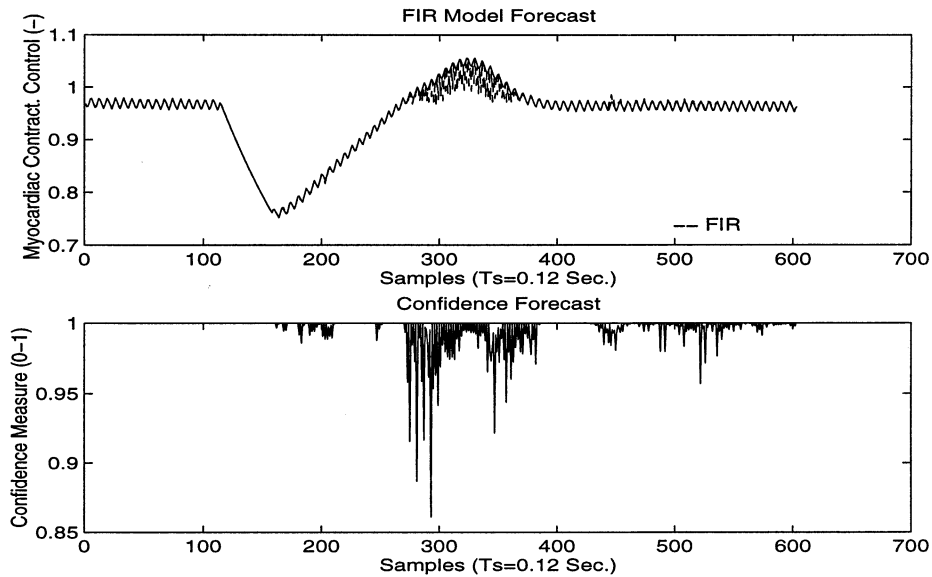


Fig. 13. FIR estimation of the confidence in its ability to forecast the myocardial contractility controller model.

neighbors that were computed in order to estimate the membership function value of the new output, Eq. (20). The measure used in FIR to evaluate the confidence in a prediction made is a proximity measure based on the proximity of the input states of the five nearest neighbors to the new input state.

An average distance to the five nearest neighbors can be computed as:

$$d_{\text{conf}} = \sum_{j=1}^5 \omega_{\text{rel}_j} \cdot d_j \quad (28)$$

The largest possible value of the average distance, given the chosen granularity of the discretization, can be calculated as:

$$d_{\text{conf}_{\text{max}}} = \sqrt{\sum_{i=1}^N (n_{\text{cl}_i} - 1)^2} \quad (29)$$

where n_{cl_i} is the number of classes used in the fuzzification of the i th input variable.

Finally, the confidence is evaluated as:

$$\text{conf} = 1.0 - \frac{d_{\text{conf}}}{d_{\text{conf}_{\text{max}}}} \quad (30)$$

conf is a quality measure, i.e. a real-valued number in the range of (0.0–1.0).

The knowledge provided by the confidence estimator can be further exploited. It is possible to make parallel predictions using two different masks, e.g. the optimal mask and one or two suboptimal masks of high quality. Each prediction will be accompanied by a measure of confidence. It would make sense to choose, at each point in time, as the final output of the prediction algorithm, the one prediction that is accompanied by the highest confidence measure. Thereby, it should be possible to eliminate the poor forecasting segments almost entirely. However, this has not been tried yet.

8. Conclusions

In this paper, a portion of the human CNS control has been modeled using inductive modeling techniques, namely the portion that is responsible for the functioning of the heart, and, more generally, the blood transport through the body.

Five controller models, for a single patient, describing different control actions related to cardiovascular control have been identified separately using the NARMAX quantitative inductive modeling technique and the FIR qualitative inductive modeling approach (Table 4).

It was shown that the FIR methodology is capable of capturing dynamic behavior of systems much more accurately than the NARMAX approach. The resulting NARMAX models are much simpler, but considerably less robust than their FIR cousins.

The most important characteristic of the FIR models is their self-assessment capability. FIR models have a way of knowing the quality of their own predictions, a fact that increases dramatically the robustness of the forecasting process as well as the confidence that the user should have in the predictions made.

NARMAX models are parametric models. Once their structure has been determined, the five NARMAX models form a set of algebraic equations containing a bunch of parameters. Thus, NARMAX models can be easily optimized by any off-the-shelf curve-fitting algorithm. Training a NARMAX model consists of two separate steps: (i) determining the optimal equation structure; and (ii) optimizing the parameters of the selected structure. Most of the computational effort is spent on the optimization. Thus, designing a NARMAX model is predominantly an optimization problem.

FIR models are non-parametric models. Training a FIR model also consists of two steps: (i) determining the qualitative equation structure, i.e. the optimal mask; and (ii) composing a historical data base for holding the previous experience, i.e. the previously observed input/output patterns. Designing a FIR model is a synthesis procedure, not an optimization problem. Hence, although it is fairly simple and fast to set up a FIR model,

the methodology does not offer an easy means for post-optimizing it.

The NARMAX approach has the advantage of being naturally adaptive, i.e. it lends itself to post-optimization. This does not hold true for the FIR model. However, since setting up a new FIR model is usually a simple and fast process, post-optimization is not truly needed. When a FIR model needs to be modified, it is acceptable to simply identify a new model, since this procedure does not require much time. Also, some adaptation would be possible in the FIR approach as well, not by optimizing parameters, but by updating the experience data base on the fly.

The NARMAX model is much simpler to implement and does not require an experience data base as is the case for the FIR model. Thus, the NARMAX model needs much less memory, and also the simulation is somewhat faster than using the FIR model. However, the additional implementational effort of the FIR methodology goes hand in hand with a much increased flexibility and capability of replicating arbitrarily nonlinear system behavior.

Finally, the self-assessment capability of FIR presents a very strong argument in favor of this approach.

To summarize, it has been demonstrated that the qualitative non-parametric FIR model synthesis technique is a powerful tool for the identification of inductive models of the five CNS controllers. It compares favorably with the quantitative parametric NARMAX model optimization technique when used for such purpose.

The FIR methodology is definitely preferable to NARMAX in the context of soft-systems modeling and simulation due to its self-assessment capability. Due to the lack of meta-knowledge related to these systems, the end user is usually quite ill-equipped for judging the correctness of the simulation results obtained, and it should not be left to him or her to do so. The robustness of the simulation engine is paramount to instil trust in the end user of the tool.

The computational complexity of the FIR methodology is polynomial, except for the exhaustive search used originally as part of its modeling stage. However, suboptimal search strategies

Table 4
Comparison of MSE errors obtained by the NARMAX and FIR controller models

Controller	NARMAX ^a (%)	FIR (%)
Heart rate	9.80	1.37
Peripheric res.	14.89	1.49
Myocardiac cont.	17.21	1.41
Venous tone	16.89	1.47
Coronary res.	31.69	0.09

^a Notice that the number of terms of each NARMAX model differs as explained in the text.

of polynomial complexity have recently been implemented and experimented with as described in [15,16]. Using these new search strategies, it has become quite feasible to apply FIR to modeling problems involving many input variables and a fairly large mask depth.

Appendix A. Differential equations of the hemodynamical and the central nervous system models

In this appendix the differential equations of the hemodynamical model and the differential equations of the CNS control model are described.

A.1. The hemodynamical model

The blood flow through the complex network of vessels in the circulatory system has been described using 15 compartments distributed in the heart, thorax and abdomen. Each compartment is an elastic reservoir with lumped hydrodynamic parameters representing the properties of blood vessel collection. In order to simulate the Valsalva maneuver, intrathoracic and intraabdominal pressures are added to the pressure of the arterial and venous compartments situated in the thorax and abdomen, respectively.

The heart, composed of four chambers (right and left atrium, and right and left ventricle), is modeled as a set of four unidirectional pumps. The duration of the systole and diastole of each chamber are described by the following equations:

$$T_{AS} = 0.09 \cdot T_{TOT} + 0.1 \quad (31)$$

$$T_{AV} = T_{AS} - 0.04 \quad (32)$$

$$T_{VS} = 0.20 \cdot T_{TOT} + 0.16 \quad (33)$$

where T_{AS} is the duration of the atrial systole, T_{AV} is the time between the onset of atrial systole and the onset of ventricular systole, T_{VS} is the duration of ventricular systole, and T_{TOT} is the total cardiac cycle.

The active pressure of each heart chamber is given by Eq. (34), where $V(t)$ is the time-varying volume of each chamber, V_u is its unstressed volume and $E(t)$ is its time-varying elastance [9].

$$P(t) = E(t) \cdot [V(t) - V_u] \quad (34)$$

A half-sinusoidal pattern is used in the elastance function for the four heart chambers during the systole, and a constant is used throughout the diastole [4]. Eq. (35) is the sinusoid for the right and left atria during the time t_i of a cardiac cycle, and Eq. (36) is the sinusoid for the right and left ventricles.

$$X(t) = \begin{cases} \sin(\pi t_i / T_{AS}) & 0 \leq t_i < T_{AS} \\ 0, & T_{AS} \leq t_i < T_{TOT} \end{cases} \quad (35)$$

$$Y(t) = \begin{cases} 0 \\ \sin[\pi(t_i - T_{AV}) / T_{VS}] \\ 0 \end{cases},$$

$$\begin{aligned} 0 &\leq t_i \leq T_{AV} \\ T_{AV} &< t_i < (T_{AV} + T_{VS}) \\ (T_{AV} + T_{VS}) &\leq t_i < T_{TOT} \end{aligned} \quad (36)$$

The basic description of the elastance, pressure and volume for the right atrium are given by Eqs. (37) and (38) and Eq. (39), where the suffixes RA and RV denote right atrium and right ventricle, respectively.

$$E_{RA}(t) = X(t) \cdot (E_{RAS} - E_{RAD}) + E_{RAD} \quad (37)$$

$$P_{RA}(t) = E_{RA}(t) \cdot [V_{RA}(t) - V_{uRA}] + P_{ITH}(t) \quad (38)$$

$$V_{RA}(t) = \int_0^t [F_{RA}(t) - F_{RARV}(t)] \cdot dt + V_{RA}(0) \quad (39)$$

In a similar manner, equations can be written describing the dynamics occurring in the left atrium.

The elastance, pressure, and volume of the left ventricle are modeled by the following equations:

$$E_{LV}(t) = Y(t) \cdot (E_{LVS} - E_{LVD}) + E_{LVD} \quad (40)$$

$$P_{LV}(t) = E_{LV}(t) \cdot [V_{LV}(t) - V_{uLV}] + P_{ITH}(t) \quad (41)$$

$$V_{LV}(t) = \int_0^t [F_{LALV}(t) - F_{LVA}(t)] \cdot dt + V_{LV}(0) \quad (42)$$

where the suffixes LA and LV denote left atrium and left ventricle, respectively. Similar equations are developed for the right ventricle describing the flow through the pulmonary valve.

The systemic arteries have been modeled taking inertial effects and wall viscoelasticity into account. The set of equations obtained by Beneken and De Wit [12] to describe an arterial compartment are presented below:

$$\Delta P(t) = R \cdot F_{\text{out}}(t) + L \cdot dF_{\text{out}}(t)/dt \quad (43)$$

$$V(t) = \int_0^t [F_{\text{in}}(t) - F_{\text{out}}(t)] \cdot dt + V(0) \quad (44)$$

$$P(t) = [V(t) - V_u]/C + R_w \cdot dV(t)/dt + P_p(t) \quad (45)$$

where $\Delta P(t)$ is the difference of pressures between two consecutive compartments, $F_{\text{out}}(t)$ is the outflow of the compartment, $F_{\text{in}}(t)$ is the flow into the compartment, and V_u is the unstressed volume of the pool. R is the resistance between them, L is the inertia, C is the compliance and R_w is equivalent to the wall viscosity of the pool. The intrathoracic or intraabdominal pressure is $P_p(t)$, depending on where the compartment is placed.

The pressure of the pulmonary arterial compartment is described similar Eq. (45), which models the pressure in an arterial compartment, but without considering the effects of the R_w resistance.

The systemic veins have been modeled as a non-linear high-compliant and collapsible system. The following equation describes a venous compartment:

$$P(t) = [V(t) - V_u]/C \quad (46)$$

The venous collapse is assumed to occur whenever the volume $V(t)$ of a compartment becomes less than the unstressed volume V_u . Based on the work of Snyder and Rideout [7], the compliance of the veins is assumed to be expressed by Eq. (47).

$$C = \begin{cases} C_N, & V(t) \geq V_u \\ 20 \cdot C_N, & V(t) < V_u \end{cases} \quad (47)$$

For $V(t) \geq V_u$, the veins are assumed to have a constant compliance C_N , using values obtained from the literature [12]. For $V(t) < V_u$, the compliance is also assumed constant, but 20 times greater. The volume $V(t)$ is calculated in an analogous manner to Eq. (44), although $F_{\text{out}}(t)$ is described by the following equations:

$$F_{\text{out}}(t) = \begin{cases} F_{\text{aux}}(t), & F_{\text{aux}}(t) \geq 0 \\ \alpha \cdot F_{\text{aux}}(t), & F_{\text{aux}}(t) < 0 \end{cases} \quad (48)$$

$$F_{\text{aux}}(t) = \Delta P(t) \cdot V^2(t) / (R \cdot V_u^2) \quad (49)$$

where the venous valves are represented by the coefficient α , and no effect of venous valves is present when $\alpha = 1$. $F_{\text{aux}}(t)$ corresponds to the flow between the arterial compartments.

The pressure difference between two consecutive compartments of the systemic peripheral circulation is described by Eq. (50):

$$\Delta P(t) = R \cdot F_s(t) \quad (50)$$

where the effects of the inertia L are not considered.

The relation between blood flow and pressure in the lungs is modeled by Eq. (51) ([12,8])

$$F_{\text{PAPV}}(t) = \begin{cases} (P_{\text{PA}}(t) - P_{\text{PV}}(t)) / R_{\text{PAPV}}, & P_{\text{PV}}(t) > 7 \cdot \text{mmHg} \\ (P_{\text{PA}}(t) - 7) / R_{\text{PAPV}}, & P_{\text{PV}}(t) \leq 7 \cdot \text{mmHg} \end{cases} \quad (51)$$

where R_{PAPV} is the peripheric resistance of the blood pulmonary circulation.

This set of differential equations completes the description of the hemodynamical quantitative model used in this article for the simulation of the cardiovascular closed-loop system. In the next section, a description of the set of differential equations that model the CNS control is presented.

A.2. The central nervous system control model

The generic equations of the mathematical model that describe the CNS control are listed in this section, (Eqs. (52)–(89)). This set of equations includes blood pressure baroreceptors at the carotid-sinus and aortic-arch. It also includes the CNS controllers for the heart rate, HR ; peripheral resistance, $Q_1(t)$; myocardial contractility, $Q_2(t)$; venous tone, $Q_3(t)$ and $Q_4(t)$; and coronary resistance, $Q_5(t)$.

The model has been based upon the work of Hyndman [10], Leaning [8] and Katona [11]. Further development of these models has resulted in the incorporation of the CNS control of the coronary flow and the parameters λ_9 and λ_{10} of the CNS control of the heart rate [1].

A.2.1. Baroreceptors of the carotid-sinus

$$f_1(t) = \begin{cases} dP_{CS}(t)/dt, & dP_{CS}(t)/dt \geq 0 \\ 0, & dP_{CS}(t)/dt < 0 \end{cases} \quad (52)$$

$$\frac{df_2(t)}{dt} = \frac{f_1(t) - f_2(t)}{\tau_2} \quad (53)$$

$$\frac{df_3(t)}{dt} = \frac{P_{CS}(t) - f_3(t)}{\tau_1} \quad (54)$$

$$f_4(t) = \lambda_1 \cdot (f_3(t) + \lambda_2 \cdot f_2(t) - \lambda_3) \quad (55)$$

$$B_{CS}(t) = \begin{cases} f_4(t), & f_4(t) \geq 0 \\ 0, & f_4(t) < 0 \end{cases} \quad (56)$$

A.2.2. Baroreceptors of the aortic-arch

$$f_5(t) = \begin{cases} dP_{AA}(t)/dt, & dP_{AA}(t)/dt \geq 0 \\ 0, & dP_{AA}(t)/dt < 0 \end{cases} \quad (57)$$

$$\frac{df_6(t)}{dt} = \frac{f_5(t) - f_6(t)}{\tau_2} \quad (58)$$

$$\frac{df_7(t)}{dt} = \frac{P_{AA}(t) - f_7(t)}{\tau_1} \quad (59)$$

$$f_8(t) = \lambda_1 \cdot [f_7(t) + \lambda_2 \cdot f_6(t) - \lambda_3] \quad (60)$$

$$B_{AA}(t) = \begin{cases} f_8(t), & f_8(t) \geq 0 \\ 0, & f_8(t) < 0 \end{cases} \quad (61)$$

The baroreceptors monitor carotid-sinus blood pressure $P_{CS}(t)$ and aortic-arch pressure $P_{AA}(t)$, and convey information to the CNS. The two baroreceptors are modeled with the same block configuration, as is described in the previous equations. In this way, baroreceptors outputs $B_{CS}(t)$ and $B_{AA}(t)$ are given as a positive linear combination. It is a combination of the positive time derivative of pressure (dP^+/dt) filtered by a first-order system, the pressure filtered by another first-order system, and a threshold pressure λ_3 below which firing does not occur. The average contribution of the positive-pressure derivative term over one cardiac cycle is given by λ_2 .

The linear combination of carotid-sinus and aortic-arch baroreceptors outputs, $B_{CS}(t)$ and $B_{AA}(t)$ respectively, is the effective input, $B(t)$, for the CNS, and is given by the following equation:

$$B(t) = \lambda_4 \cdot B_{CS}(t) + (1 - \lambda_4) \cdot B_{AA}(t) \quad (62)$$

The information from the CNS input function $B(t)$ to the controlled heart rate, HR , is transmitted by two regions characterized by the levels of the monitored pressures. The differential equations associated to the heart rate controller follow.

A.2.3. Heart rate controller

$$u_1(t) = \begin{cases} \lambda_5 \cdot B(t) - \lambda_6, & \lambda_5 \cdot B(t) \geq \lambda_6 \\ 0, & \lambda_5 \cdot B(t) < \lambda_6 \end{cases} \quad (63)$$

$$\tau_3(t) = \begin{cases} \lambda_7, & du_1(t)/dt \geq 0 \\ \lambda_8, & du_1(t)/dt < 0 \end{cases} \quad (64)$$

$$\frac{du_2(t)}{dt} = \frac{u_1(t) - u_2(t)}{\tau_3} \quad (65)$$

$$u_3(t) = \begin{cases} \lambda_{11}, & B(t) \geq \lambda_{11} \\ B(t), & B(t) < \lambda_{11} \end{cases} \quad (66)$$

$$\frac{du_4(t)}{dt} = \frac{u_3(t) - u_4(t)}{\tau_4} \quad (67)$$

$$\frac{du_5(t)}{dt} = \frac{u_4(t) - u_5(t)}{\tau_5} \quad (68)$$

$$u_6(t) = \lambda_9 \cdot [u_2(t) + u_5(t)] + \lambda_{10} \quad (69)$$

$$T_{TOT}(t) = \begin{cases} 2.0, & u_6(t) \geq 2.0 \\ u_6(t), & 0.3 \leq u_6(t) < 2.0 \\ 0.3, & u_6(t) < 0.3 \end{cases} \quad (70)$$

One region, $u_2(t)$, is integrated by a first-order system that filters the input function $B(t)$ when elevated blood pressures are present. The other region, $u_5(t)$, concerns the low blood pressures, and its dynamics have been approximated by a second-order system. The output of this controller is a linear combination of the responses of the two regions and a constant level λ_{10} . The total cardiac cycle T_{TOT} is obtained by subjecting the controller output to a constraint.

A.2.4. Peripheral resistance controller

The differential equations associated to the peripheral resistance controller follow.

$$S_1(t) = \begin{cases} \lambda_{12}, & B(t) \geq \lambda_{14} \\ \lambda_{13}, & B(t) < \lambda_{14} \end{cases} \quad (71)$$

$$\frac{dS_2(t)}{dt} = \frac{S_1(t) - S_2(t)}{\tau_6} \quad (72)$$

$$\frac{dS_3(t)}{dt} = \frac{S_1(t) - S_3(t)}{\tau_7} \quad (73)$$

$$Q_1(t) = (1 - \lambda_{15}) \cdot S_2(t) + \lambda_{15} \cdot S_3(t) \quad (74)$$

The dynamics of the peripheral resistance controller feature an on-off element that produces a bang-bang action, $S_1(t)$. This response is divided into two parallel paths, $S_2(t)$, and $S_3(t)$, where the dynamics are approximated by a first-order system. The linear combination of these two paths represents a continuously varying estimate of the peripheral resistance controller, $Q_1(t)$. This control modifies all peripheral blood flow in the following manner:

$$F_{\text{out}}(t) = \Delta P(t)/(R \cdot Q_1) \quad (75)$$

A.2.5. Myocardial contractility controller

A series path formed by an on-off element and a first-order system approximates the dynamics of the myocardial contractility controller, $Q_2(t)$. The control is done directly on the systolic elastances of the four heart chambers. The differential equations that describe the model are presented below:

$$r_1(t) = \begin{cases} \lambda_{16}, & B(t) \geq \lambda_{18} \\ \lambda_{17}, & B(t) < \lambda_{18} \end{cases} \quad (76)$$

$$\frac{dQ_2(t)}{dt} = \frac{r_1(t) - Q_2(t)}{\tau_8} \quad (77)$$

A.2.6. Venous tone controller

The dynamics of the venous tone control are similar to those of the myocardial contractility control. Two venous controls are considered, Q_3 and Q_4 .

$$h_1(t) = \begin{cases} \lambda_{19}, & B(t) \geq \lambda_{21} \\ \lambda_{20}, & B(t) < \lambda_{21} \end{cases} \quad (78)$$

$$\frac{dh_2(t)}{dt} = \frac{h_1(t) - h_2(t)}{\tau_9} \quad (79)$$

$$Q_3(t) = 1 + \lambda_{22} \cdot [h_2(t) - 1] \quad (80)$$

$$Q_4(t) = 1 + \lambda_{23} \cdot [h_2(t) - 1] \quad (81)$$

Q_3 and Q_4 modify the venous pressure in the following way:

$$P(t) = [V(t) - V_u/Q_4] \cdot Q_3/C \quad (82)$$

where Q_3 controls the compliance and Q_4 the unstressed volume.

A.2.7. Coronary resistance controller

A mathematical model of the coronary resistance control has been developed in order to improve the coronary blood flow simulation. The model considers an on-off element with a dead zone and hysteresis, $g_1(t)$.

The dynamics of this controller are completed by the combination of two branches, each approximated by a first-order system, $g_2(t)$ and $g_3(t)$. The time constants τ_{10} and τ_{11} of the first-order system are similar to the ones presented in the peripheral resistance controller.

$$\frac{dg_2(t)}{dt} = \frac{g_1(t) - g_2(t)}{\tau_{10}} \quad (83)$$

$$\frac{dg_3(t)}{dt} = \frac{g_1(t) - g_3(t)}{\tau_{11}} \quad (84)$$

$$Q_5(t) = (1 - \lambda_{31}) \cdot g_2(t) + \lambda_{31} \cdot g_3(t) \quad (85)$$

When an on-off element with a dead zone and hysteresis is considered, the following equations are used:

If $g_1(0) = \lambda_{30}$ then,

$$g_1(t) = \begin{cases} \lambda_{28}, & B(t) \geq \lambda_{27} \\ \lambda_{29}, & \lambda_{25} \leq B(t) < \lambda_{27} \\ \lambda_{30}, & B(t) < \lambda_{25} \end{cases} \quad (86)$$

If $g_1(0) = \lambda_{28}$ then:

$$g_1(t) = \begin{cases} \lambda_{28}, & B(t) \geq \lambda_{26} \\ \lambda_{29}, & \lambda_{24} \leq B(t) < \lambda_{26} \\ \lambda_{30}, & B(t) < \lambda_{24} \end{cases} \quad (87)$$

In certain cases, the effects of the dead zone do not appear, and therefore, a single on-off element with hysteresis may be useful, and the following equations apply:

If $g_1(0) = \lambda_{30}$ then:

$$g_1(t) = \begin{cases} \lambda_{28}, & B(t) \geq \lambda_{27} \\ \lambda_{30}, & B(t) < \lambda_{27} \end{cases} \quad (88)$$

If $g_1(0) = \lambda_{28}$ then:

$$g_1(t) = \begin{cases} \lambda_{28}, & B(t) \geq \lambda_{24} \\ \lambda_{30}, & B(t) < \lambda_{24} \end{cases} \quad (89)$$

References

- [1] M. Vallverdú, C. Crexells, P. Caminal, Cardiovascular responses to intrathoracic pressure variations in coronary disease patients: a computer simulation, *Technol. Health Care* 2 (1994) 119–140.
- [2] M. Vallverdú, Modelado y simulacion del sistema de control cardiovascular en pacientes con lesiones coronarias, PhD dissertation, Universitat Politècnica de Catalunya, Barcelona, 1993.
- [3] F.E. Cellier, A. Nebot, F. Mugica, A. De Albornoz, Combined qualitative/quantitative simulation models of continuous-time processes using fuzzy inductive reasoning techniques, *Int. J. Gen. Syst.* 24 (1-2) (1995) 95–116.
- [4] A. Nebot, F.E. Cellier, D.A. Linkens, Synthesis of an anaesthetic administration system using fuzzy inductive reasoning, *Artif. Intell. Med.* 8 (1996) 1.
- [5] J.E. Beneken, V.C. Rideout, The use of multiple models in cardiovascular system studies: transport and perturbation methods, *IEEE Trans. Biomed. Eng.* 15 (1996) 4.
- [6] K. Sagawa, L. Maughan, H. Suga, K. Sunagawa, Cardiac Contraction and the Pressure–Volume Relationship, Oxford University Press, NY, 1988.
- [7] M.F. Snyder, V.C. Rideout, Computer simulation studies of the venous circulation, *IEEE Trans. Biomed. Eng.* 16 (1969) 325–334.
- [8] M.S. Leaning, H.E. Pullen, E.R. Carson, L. Finkelstein, Modelling a complex biological system: the human cardiovascular system, *Trans. Inst. Meas. Control* 5 (1983) 71–86.
- [9] H. Suga, K. Sagawa, Instantaneous pressure–volume relationships and their ratio in the excised, supported canine left ventricle, *Circ. Res.* 53 (1974) 117–126.
- [10] P.W. Hyndman, A digital simulation of the human cardiovascular system and its use in the study of sinus arrhythmia, PhD thesis, Imperial College, University of London, 1970.
- [11] P.G. Katona, O. Barnett, W.D. Jackson, Computer simulation of the blood pressure control of the heart period, in: P. Kezdi (Ed.), *Baroreceptors and Hypertension*, Pergamon, Oxford, 1967, pp. 191–199.
- [12] J.E.W. Beneken, B. De Wit, A physical approach to hemodynamic aspects of the human cardiovascular system, in: E.B. reeve, A.C. Guyton (Eds.), *Physical Bases of Circulatory Transport*, W.B. Saunders, Philadelphia, 1967.
- [13] G.J. Klir, *Architecture of Systems Problem Solving*, Plenum Press, New York, 1985.
- [14] MATLAB: High performance numeric computation and visualization software-users guide, the MathWorks, Cochituate Place, Natick, MA, 1993.
- [15] A. Nebot, A. Jerez, Assessment of classical search techniques for identification of fuzzy models, *EUFIT'97: 5th European Congress on Intelligent Techniques and Soft Computing*, Aachen, Germany, 1997, pp. 904–909, ISBN: 3-89653-200-6.
- [16] A. Jerez, A. Nebot, Genetic algorithms versus classical search techniques for identification of fuzzy models, *EUFIT'97: 5th European congress on Intelligent Techniques and Soft Computing*, Aachen, Germany, 1997, pp. 769–773, ISBN: 3-89653-200-6.
- [17] A. Law, D. Kelton, *Simulation Modeling and Analysis*, 2nd ed., McGraw-Hill, New York, 1990.
- [18] D. Li, F.E. Cellier, Fuzzy measures in inductive reasoning, *Proc. 1990 Winter Simulation Conference*, New Orleans, LA, 1990, pp. 527–538.
- [19] F. Mugica, F.E. Cellier, A new fuzzy inferencing method for inductive reasoning, *Proc. Int. Symp. on Artificial Intelligence*, Monterrey, Mexico, 1993, pp. 372–379.
- [20] F.E. Cellier, *Continuous System Modeling*, Springer-Verlag, New York, 1991.
- [21] A. Nebot, Qualitative modeling and simulation of biomedical systems using fuzzy inductive reasoning, PhD dissertation, Universitat Politècnica de Catalunya, Barcelona, 1994.
- [22] MGA, ACSL: *Advanced Continuous Simulation Language—Reference Manual*, 10th ed., Mitchell and Gauthier, Concord, MA, 1991.